Modeling the Photosynthetic Water Oxidation Center: Chloride/Bromide Incorporation and Reversible Redox Processes in the Complexes $Mn_4O_3X(OAc)_3(dbm)_3$ (X = Cl, Br) and $(pyH)_3[Mn_4O_3Cl_7(OAc)_3]$

Sheyi Wang, Hui-Lien Tsai, Eduardo Libby,† Kirsten Folting, William E. Streib, David N. Hendrickson,* and George Christou*

Department of Chemistry and Molecular Structure Center, Indiana University, Bloomington, Indiana 47405-4001, and Department of Chemistry 0358, University of California at San Diego, La Jolla, California 92093-0358

Received February 8, 1996[⊗]

Synthetic procedures are described that allow conversion of $[Mn_4O_2(OAc)_6(py)_2(dbm)_2]$ (**1**, dbmH = dibenzoylmethane) to $[Mn_4O_3X(OAc)_3(dbm)_3]$ (X = Cl, **2**; X = Br, **3**). Treatment of **1** with NBu^n_4Cl in CH_2Cl_2 or hot MeCN leads to **2** in 5−8% and 35−43% yields (based on dbm), respectively. A higher yield (∼88%) is obtained by treating **1** with 4 equiv of Me_3SiCl in CH_2Cl_2. An analogous procedure with 4 equiv of Me_3SiBr in CH_2Br_2 gives **3** in 55% yield. Complexes **2** and **3** are isomorphous, monoclinic space group $P2_1/n$, $T = -155$ °C, $Z = 4$. For **2**, $a = 13.900(3)$, $b = 22.038(5)$, and $c = 16.518(5)$ Å and $\beta = 107.80(1)°$; for **3**, $a = 13.644(2)$, $b = 22.190(4)$, and $c = 16.548(3)$ Å, and $\beta = 106.64(1)°$. The structures were solved by direct methods (MULTAN78) and refined on F to $R(R_w)$ values of 7.85 (7.38) and 7.37 (6.89)% using 2267 and 2809 unique reflections with $F > 2.33\sigma(F)$ for **2** and **3**, respectively. Treatment of $[Mn_3O(OAc)_6(py)_3](ClO_4)$ in MeCN with Me_3SiCl followed by addition of H_2O and acetic acid results in crystallization of $(pyH)_3[Mn_4O_3Cl_7(OAc)_3]\cdot 2MeCN$ (**4**) in 75% yield (based on Mn). Complex **4** crystallizes in monoclinic space group $C2/c$ with the following cell parameters at −157 °C: $a = 37.420(5)$, $b = 13.752(1)$, and $c = 16.139(2)$ Å, $\beta = 110.33(1)$, $V = 7787.9$ Å^3, and $Z = 8$. The structure was solved by direct methods (MULTAN78) and refined on F to $R(R_w)$ values of 5.74 (5.78)% using 2612 unique reflections with $F > 3.0\sigma(F)$. The complexes possess a $[Mn_4(\mu_3\text{-}O)_3(\mu_3\text{-}X)]$ distorted cubane core and a $3Mn^{III},Mn^{IV}$ trapped-valence oxidation-state description. Three AcO^- groups bridge each $Mn^{III}Mn^{IV}$ pair, and a chelating dbm^- (**2** and **3**) or two Cl^- ions (**4**) on each Mn^{III} complete peripheral ligation. The pyridinium cations of **4** are involved in hydrogen-bonding interactions with the $\mu_3\text{-}O^{2-}$ and the terminal Cl^- ions of the anion. Variable-temperature solid-state magnetic susceptibility studies show that the magnetic properties of **2** and **3** are very similar: μ_{eff} values steadily rise from ∼9 μ_B at room temperature to ∼10 μ_B at 30.0 K and then drop rapidly to ∼9.5 μ_B at 5 K. Fitting of the experimental data for the two complexes to the appropriate theoretical equation yield the following fitting parameters, in the format **2**/**3**: $J = J(Mn^{III}\cdots Mn^{IV}) = -28.4/-30.1$ cm^{-1}, $J' = J(Mn^{III}\cdots Mn^{III}) = +8.3/+7.4$ cm^{-1}, and $g = 1.98/2.03$. Both **2** and **3** have $S = {}^9/_2$ ground states that are well-separated (∼180 cm^{-1}) from an $S = {}^7/_2$ first excited state. The ground state was confirmed by magnetization vs magnetic field studies at several fields and temperatures; fitting of the data allowed the zero-field splitting parameter D to be determined for both complexes. The magnetochemical properties of **4** are very similar to those of **2** and **3**, and the fitting parameters were $J = -29.1$ cm^{-1}, $J' = +10.2$ cm^{-1}, and $g = 1.97$, giving an $S = {}^9/_2$ ground state and showing that the hydrogen-bonding interactions of the $\mu_3\text{-}O^{2-}$ ions do not cause a significant change to the exchange parameters or to the electronic structure of the $[Mn_4O_3Cl]^{6+}$ core. ^{1}H NMR spectra of **2**−**4** in $CDCl_3$ or CD_3CN solution at ∼23 °C are similar and show that the Mn_4 complexes retain their solid-state structure on dissolution in this solvent. X-band EPR spectra of **2** and **3** in CH_2Cl_2/toluene (1:1) glasses at 5 K are also extremely similar, with three main features at $g = 11.0$, 5.2, and 1.96. Cyclic voltammetry at 100 mV/s and differential pulse voltammetry at 5 mV/s show that both **2** and **3** support a reversible oxidation and two reductions, the first of which is reversible. The reversible processes are at 1.09/1.06 and −0.25/−0.21 V vs ferrocene and show that the $[Mn_4O_3X]$ core can exist at three oxidation levels spanning the $4Mn^{III}$ to $2Mn^{III}$, $2Mn^{IV}$ range. The combined results from **2** and **3** show that the identity of X has minimal influence on the resultant structures, magnetic properties, ^{1}H NMR and EPR spectral properties, or the redox behavior. Such observations are of interest with regard to the ability of Br^- to successfully substitute for Cl^- at the photosynthetic water oxidation center and thus maintain the activity of the tetranuclear Mn aggregate toward oxygen evolution.

Introduction

Water oxidation to oxygen gas by the photosynthetic apparatus of green plants and cyanobacteria represents the origin of this gas in the atmosphere and provides a source of protons and reducing equivalents for photosynthesis.[1,2] The site of water oxidation is a tetranuclear, oxide-bridged, manganese cluster with primarily O-based (carboxylate) and low levels of N-based (imidazole) peripheral ligation provided by amino acid side-chain groups (Asp, Glu, His).[1,2] This redox-active water oxidizing complex (WOC) acts as an electron donor to photo-

† Present address: Department of Chemistry, University of Costa Rica, Costa Rica.

⊗ Abstract published in *Advance ACS Abstracts,* December 1, 1996.

(1) Debus, R. J. *Biochim. Biophys. Acta* **1992**, *1102*, 269 and references cited therein.
(2) *Manganese Redox Enzymes*; Pecoraro, V. L., Ed.; Verlag Chemie: Weinheim, Germany, 1992.

S0020-1669(96)00134-6 CCC: $12.00

system II (P680) via the intermediacy of redox-active tyrosine Y_z. When four electrons have been transferred, in four one-electron steps, the WOC is reduced back to its lowest oxidation level by the oxidation of water to O_2 and four protons, and is ready for recycling. The oxidation states of the WOC involved in the catalytic cycle are called the S_n states ($n = 0-4$), the subscript n referring to the number of reducing equivalents transferred *vis-à-vis* the most reduced state S_0.[3]

One intriguing property of the WOC is its absolute requirements for two or three Ca^{2+} ions and several Cl^- ions for activity.[1,2,4,5] The precise roles of these cofactors are unknown. Restricting further discussion to Cl^-, this ion has been suggested to be bound to the Mn, bound to a nearby site such as Ca^{2+}, involved in charge neutralization, or involved in some other function not involving binding to Mn.[4] Interestingly, inactive preparations that lack Cl^- can be reactivated by addition of Br^-.[4,5] Whatever the function of Cl^- is, it thus appears that it can also be carried out by Br^-. Other anions will also restore activity, but only to a much lesser extent.[4,5]

The precise structure and mechanism of action of the WOC remains unknown. However, extended X-ray absorption fine structure (EXAFS) data have proven extremely useful in providing insights into the structure of the WOC.[6-8] Mn K-edge EXAFS data have revealed that the four Mn atoms are disposed in an asymmetric fashion and are bridged by O^{2-} ions; there are Mn···Mn separations of 2.74(2) Å, characteristic of a bis-O^{2-}-bridged Mn_2 pair (i.e., $[Mn(\mu\text{-}O)_2Mn]$ subfragments) as well as longer Mn···Mn separations of 3.1−3.4 Å characteristic of Mn atoms bridged by (at most) only one oxide ion. Low levels of Cl^- ligation to the WOC (i.e., one per Mn_4) cannot be ruled out by the EXAFS data.[6] EXAFS data for plants and cyanobacteria are very similar.[6d]

De Rose *et al.*[6d] recently considered topological possibilities for $[Mn_4O_x]$ cores that would be consistent with their most recent EXAFS data and presented 10 structural possibilities ranging from a linear disposition of four Mn atoms to a variety of more condensed arrangements. The authors stated that they prefer a "dimer-of-dimers" topology, but in principle any of the 10 possibilities could be present in the WOC.

As part of our program to obtain synthetic analogues of the WOC, we have developed procedures to a number of tetranuclear, oxide-bridged Mn carboxylate clusters.[9-11] One type of complex that we have prepared contains the core shown below,[10,11]

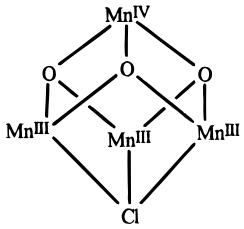

which is best described as a "tetra-face-capped Mn_4 trigonal prism" or, for convenience, a (highly) "distorted cubane". The core has C_{3v} virtual symmetry with $Mn^{III}\cdots Mn^{IV}$ and $Mn^{III}\cdots Mn^{III}$ distances of ~2.81 and ~3.3 Å, respectively, emphasizing the severe deviation from true cubane (T_d) symmetry. The $[Mn_4O_3]$ trigonal-pyramidal unit was one of the topologies presented by De Rose *et al.*[6d] in their considerations of units consistent with WOC EXAFS data.

Our initial products with the above $[Mn_4O_3Cl]^{6+}$ core were the complexes $[Mn_4O_3Cl_4(O_2CR)_3(py)_3]$ (R = various), and related species,[10] containing bridging RCO_2^- groups across each $Mn^{III}Mn^{IV}$ pair and terminal Cl^- and py groups on each Mn^{III}. The high Cl^- content of these complexes was clearly incompatible with available data on the WOC, and therefore we have since sought to alter the peripheral ligation at the Mn^{III} sites of the $[Mn_4O_3Cl]$ core. Although carboxylate variation is readily accomplished by ligand substitution reactions of preformed $[Mn_4O_3Cl_4(OAc)_3(py)_3]$ with more acidic carboxylic acids (e.g., benzoic acid),[11] variation of the terminal ligands at the Mn^{III} sites by ligand substitution reactions on preformed $[Mn_4O_3Cl_4(OAc)_3(py)_3]$ has proven difficult, and alternate procedures have been sought.

We herein report the development of a new type of $[Mn_4O_3Cl]^{6+}$ complex containing completely O-based peripheral ligation, namely, carboxylate and dbm^- (dbmH = dibenzoylmethane) groups. In addition, we show that this ligation environment supports reversible redox chemistry in both the oxidizing and reducing directions, behavior not seen with our previous family of $[Mn_4O_3Cl]^{6+}$ complexes. Further, we have successfully sought the substitution of Br^- for Cl^- in the $[Mn_4O_3Cl]^{6+}$ core to probe the effect of the halide identity on the properties of these complexes and to thereby gain some insight into the known ability of Br^- to substitute for Cl^- in the WOC. We also include, for comparison purposes, the new complex $(pyH)_3[Mn_4O_3Cl_7(OAc)_3]$ possessing only Cl^- terminal ligation at the Mn^{III}. Portions of this work have been previously communicated.[12,13]

Experimental Section

Syntheses. Unless otherwise noted, all manipulations were performed under aerobic conditions at ambient temperature using reagents

(3) Kok, B.; Forbush, B.; McGloin, M. P. *Photochem. Photobiol.* **1970**, *11*, 457.
(4) Yocum, C. F. in ref 2, Chapter 4, pp 71−84 and references cited therein.
(5) (a) Kelley, P. M.; Izawa, S. *Biochim. Biophys. Acta* **1978**, *502*, 198. (b) Homann, P. H. *Biochim. Biophys. Acta* **1988**, *88*, 194. (c) Theg, S.; Homann, P. H. *Biochim. Biophys. Acta* **1982**, *679*, 221. (d) Theg, S. M.; Jursinic, P. M.; Homann, P. H. *Biochim. Biophys. Acta* **1984**, *766*, 636. (e) Itoh, S.; Yerkes, C. T.; Koike, H.; Robinson, H. H.; Crofts, A. R. *Biochim. Biophys. Acta* **1984**, *766*, 612.
(6) (a) Sauer, K.; Yachandra, V. K.; Britt, R. D.; Klein, M. P. in ref 2, Chapter 8, pp 141−175 and references cited therein. (b) Liang, W.; Latimer, M. J.; Dau, H.; Roelofs, T. A.; Yachandra, V. K.; Sauer, K.; Klein, M. P. *Biochemistry* **1994**, *33*, 4923. (c) Yachandra, V. K.; Guiles, R. D.; McDermott, A. E.; Cole, J. L.; Britt, R. D.; Dexheimer, S. L.; Sauer, K.; Klein, M. P. *Biochemistry* **1987**, *26*, 5974. (d) DeRose, V. J.; Mukerji, I.; Latimer, M. J.; Yachandra, V. K.; Sauer, K.; Klein, M. P. *J. Am. Chem. Soc.* **1994**, *116*, 5239. (e) Guiles, R. D.; Zimmermann, J.-L.; McDermott, A. E.; Yachandra, V. K.; Cole, J. L.; Dexheimer, S. L.; Britt, R. D.; Wieghardt, K.; Bossek, U.; Sauer, K.; Klein, M. P. *Biochemistry* **1990**, *29*, 471.
(7) (a) Penner-Hahn, J. E.; Fronko, R. M.; Pecoraro, V. L.; Yocum, C. F.; Betts, S. D.; Bowlby, N. R. *J. Am. Chem. Soc.* **1990**, *112*, 2549. (b) Riggs, P. J.; Mei, R.; Yocum, C. F.; Penner-Hahn, J. E. *J. Am. Chem. Soc.* **1992**, *114*, 10650.
(8) (a) Kusunoki, M.; Ono, T.; Noguchi, T.; Inoue, Y.; Oyanagi, H. *Photosynth. Res.* **1993**, *38*, 331. (b) Kusunoki, M.; Ono, T.; Matsushita, T.; Oyanagi, H.; Inoue, Y. *J. Biochem.* **1990**, *108*, 560.
(9) (a) Christou, G. *Acc. Chem. Res.* **1989**, *22*, 328. (b) Vincent, J. B.; Christmas, C.; Chang, H.-R.; Li, Q.; Boyd, P. D. W.; Huffman, J. C.; Hendrickson, D. N.; Christou, G. *J. Am. Chem. Soc.* **1989**, *111*, 2086. (c) Libby, E.; McCusker, J. K.; Schmitt, E. A.; Folting, K.; Hendrickson, D. N.; Christou, G. *Inorg. Chem.* **1991**, *30*, 3486. (d) Bouwman, E.; Bolcar, M. A.; Libby, E.; Huffman, J. C.; Folting, K.; Christou, G. *Inorg. Chem.* **1992**, *31*, 5185.
(10) Hendrickson, D. N.; Christou, G.; Schmitt, E. A.; Libby, E.; Bashkin, J. S.; Wang, S.; Tsai, H.-L.; Vincent, J. B.; Boyd, P. D. W.; Huffman, J. C.; Folting, K.; Li, Q.; Streib, W. E. *J. Am. Chem. Soc.* **1992**, *114*, 2455.
(11) Wemple, M. W.; Tsai, H.-L.; Folting, K.; Hendrickson, D. N.; Christou, G. *Inorg. Chem.* **1993**, *32*, 2025.
(12) Wang, S.; Folting, K.; Streib, W. E.; Schmitt, E. A.; McCusker, J. K.; Hendrickson, D. N.; Christou, G. *Angew. Chem., Int. Ed. Engl.* **1991**, *30*, 305.
(13) Wang, S.; Tsai, H.-L.; Streib, W. E.; Christou, G.; Hendrickson, D. N. *J. Chem. Soc., Chem. Commun.* **1992**, 1427.

and solvents as received. CH_2Cl_2 and MeCN for spectroscopic and electrochemical studies were distilled from CaH_2. The complexes $[Mn_3O(OAc)_6(py)_3](ClO_4)$[14] and $Mn_4O_2(OAc)_6(py)_2(dbm)_2$ (**1**)[12] were available from previous work.

$[Mn_4O_3Cl(OAc)_3(dbm)_3]$ (2). (a) Method 1. Solid Bu^n_4NCl (0.070 *g*, 0.25 mmol) was added to a stirred dark brown solution of complex **1** (0.30 *g*, 0.25 mmol) in CH_2Cl_2 (15 mL). The resultant solution was filtered and the filtrate layered with Et_2O (20 mL) and MeCN (10 mL). After several days, well-formed black crystals were collected by filtration, washed with Et_2O, and dried in air; yield was 5−8% based on available dbm. These crystals were suitable for X-ray diffraction studies. Anal. Calcd (Found) for $C_{51}H_{42}O_{15}ClMn_4$: C, 53.3 (52.9); H, 3.7 (3.7); Cl, 3.1 (3.3); Mn, 19.1 (18.8). Electronic spectrum in CH_2Cl_2: λ_{max}, nm (ϵ_M, L mol^{-1} cm^{-1}); 372 (65 000), 450 (7600), 488 (5470). Selected IR data (Nujol): 1589 (m), 1570 (m), 1558 (m), 1522 (s), 1346 (s), 1320 (s), 1232 (m), 1072 (m), 1026 (m), 943 (m), 763 (m), 723 (m), 686 (m), 650 (m), 613 (m), 592 (s), 576 (s), 544 (m), 530 (m), 513 (m), 470 (w) cm^{-1}.

(b) Method 2. To a hot, filtered solution of complex **1** (0.30 *g*, 0.25 mmol) in MeCN (35 mL) was added solid Bu^n_4NCl (0.070 *g*, 0.25 mmol). The resultant solution was stirred for a few minutes and then allowed to cool undisturbed to room temperature. The red-brown crystalline solid that precipitated was collected by filtration, washed with MeCN, and dried in air; the yield was 35−43% based on dbm. The IR spectrum was identical to that for material from method 1. Anal. Calcd (Found) for $C_{51}H_{42}O_{15}ClMn_4$: C, 53.3 (53.6); H, 3.7 (3.7); Cl, 3.1 (2.5); Mn, 19.1 (18.7).

(c) Method 3. To a stirred dark brown solution of complex **1** (0.60 *g*, 0.50 mmol) in CH_2Cl_2 (25 mL) was added Me_3SiCl (0.10 mL, 0.78 mmol) dropwise to give a dark red-brown solution, and the solution was then stirred for a further few minutes. Some white precipitate was removed by filtration, and the filtrate was layered with Et_2O (50 mL). After several days, black crystals and some white powder had precipitated and were collected by filtration. The white solid was readily removed by washing with a little EtOH; the crystals were further washed with Et_2O and dried in air. The yield was ∼88% based on dbm. The IR spectrum was identical to that for material from method 1. Anal. Calcd (Found) for $C_{51.6}H_{43.2}O_{15}Cl_{2.2}Mn_4$ (**2**·0.6CH_2Cl_2; FW = 1161.70): C, 51.6 (51.1); H, 3.6 (3.6); Cl, 6.49 (6.45); Mn, 18.3 (18.3). (The sample lost weight during weighing prior to analysis.)

$[Mn_4O_3Br(OAc)_3(dbm)_3]$ (3). To a stirred dark brown solution of complex **1** (0.60 *g*, 0.50 mmol) in CH_2Br_2 (20 mL) was added Me_3SiBr (0.10 mL, 0.78 mmol) dropwise to give a dark red-brown solution. This was stirred for a further few minutes and some white precipitate removed by filtration. The filtrate was layered with Et_2O (40 mL); several days later, black crystals and some white solid had appeared. These were collected by filtration, the white solid was removed by washing with EtOH, and the black crystals were washed with Et_2O and dried in air. The yield was 55% based on dbm. Anal. Calcd (Found) for $C_{51.6}H_{43.2}O_{15}Br_{2.2}Mn_4$ (**3**·$^2/_3CH_2Br_2$·$^2/_3Et_2O$; FW = 1357.27): C, 48.0 (47.9); H, 3.7 (3.5); Br, 13.7 (13.6); Mn, 16.2 (16.0). (The sample lost weight during weighing prior to analysis.) Selected IR data (Nujol): 1589 (m), 1570 (m), 1558 (m), 1520 (s), 1346 (s), 1323 (s), 1232 (m), 1072 (m), 1026 (m), 943 (m), 787 (w), 763 (m), 723 (m), 686 (m), 648 (m), 611 (m), 590 (s), 574 (s), 542 (m), 530 (m), 505 (m), 470 (w) cm^{-1}.

$(pyH)_3[Mn_4O_3Cl_7(OAc)_3]$·2MeCN (4). To a stirred, dark red-brown solution of $[Mn_3O(OAc)_6(py)_3](ClO_4)$ (0.87 *g*, 1.0 mmol) in MeCN (50 mL) was added Me_3SiCl (0.70 mL, 5.5 mmol) followed after 30 s by a solution of acetic acid (0.065 *g*, 1.08 mmol) and water (0.065 *g*, 3.6 mmol) in MeCN (5 mL). The flask was stored at −15 °C for 72 h, and this produced dark brown crystals and a small amount of colorless crystals. The solids were collected by filtration, washed with absolute EtOH (4 × 10 mL), to remove the colorless solid, and MeCN (2 × 5 mL), and dried in air. The yield was 0.50 *g* (75% based on total available Mn). The crystals were suitable for X-ray crystallography. Anal. Calcd (Found) for $C_{25}H_{33}N_5O_9Cl_7Mn_4$: C, 29.57 (29.65); H, 3.28 (3.25); N, 6.90 (6.8); Cl, 24.44 (24.7). Selected IR data (Nujol mull): 2247 (w), 1634 (m), 1559 (s), 1532 (s), 1341 (s), 1241 (w), 1200 (m), 745 (s), 679 (s), 619 (w), 575 (s), 522 (w), 498 (m). Electronic spectrum in MeCN: 256 (39.000), 304 (20,000), 566 (1210, sh) cm^{-1}.

X-ray Crystallography and Structure Solution. Data were collected on a Picker four-circle diffractometer at −155 °C; details of the diffractometry, low-temperature facilities, and computational procedures employed by the MSC are available elsewhere.[15] Small black crystals suitable for X-ray diffraction were selected from the bulk samples and transferred to the goniostat where they were cooled to −155 °C for characterization and data collection ($6° \le 2\theta \le 45°$, $+h,+k,\pm l$).

For **2** and **3**, systematic searches of a limited hemisphere of reciprocal space yielded sets of reflections that exhibited monoclinic (2/*m*) symmetry. The systematic extinctions of 0*k*0 for $k + 2n + 1$ and of *h*01 for $h + l = 2n+1$ uniquely identified both space groups as $P2_1/n$. The crystals of **2** and **3** did not diffract too strongly past $2\theta = 30°$. Plots of the standard reflections revealed no systematic trends during the data collection, and no absorption corrections were carried out. Following the usual data reduction and averaging of redundant data, 6317 (**2**) and 6295 (**3**) unique reflections were obtained. The averaging *R* values were 0.132 (**2**) and 0.068 (**3**) for 3268 and 1395 reflections, respectively, measured more than once. The structures were solved by the usual combination of direct methods (MULTAN78) and difference Fourier techniques. The four Mn atoms as well as the halogen atom were located in the initial *E* map, and the remaining atoms were located in successive difference Fourier maps phased by the already located atoms. Owing to the limited amount of strong reflections, the hydrogen atoms were introduced in fixed idealized positions for the final cycles of refinement, with thermal parameters fixed at one plus the isotropic thermal parameter of the atoms to which they were bonded. For **2**, only the Mn, Cl, and cubane core O atoms were refined anisotropically; for **3**, the Mn, Br, and *all* O atoms were refined anisotropically. Carbon atoms were refined with isotropic thermal parameters. The total number of variables was 326 (**2**) and 386 (**3**), including the scale factor and an isotropic extinction parameter. The final difference Fourier maps were essentially featureless, the largest peaks being 0.60 and 0.87 e/Å^3 for **2** and **3**, respectively. Final *R* and R_w values are listed in Table 1.

For complex **4**, a systematic search of a limited hemisphere of reciprocal space yielded a set of reflections that exhibited monoclinic symmetry (2/*m*). The systematic extinction of *hk1* for $h + k = 2n + 1$, of *h*01 for $l = 2n + 1$, and of 0*k*0 for $k = 2n + 1$ limited the choice of possible space groups to *Cc* or *C*2/*c*. The choice of the centrosymmetric space group *C*2/*c* was confirmed by the successful solution and refinement of the structure. A total of 6624 reflections (including standards and noncentered extinctions) was collected. Following the usual data reduction and averaging of equivalent reflections, a unique set of 5105 reflections was obtained. The *R* for the averaging was 0.065 for 1101 reflections observed more than once. The standard reflections collected at regular intervals during the data collection showed no significant trends. No correction for absorption was performed. The structure was determined by a combination of direct methods (MULTAN78) and Fourier techniques. The four Mn atoms and the seven Cl atoms were located in the initial *E* map, and the remainder of the non-hydrogen atoms were located in successive difference Fourier maps phased by already located atoms. The asymmetric unit also contains two molecules of solvent CH_3CN. Almost all of the hydrogen atoms were located in a later difference Fourier map and were introduced in idealized, fixed positions during the final cycles of refinement. No hydrogen atoms were located in the area of the hydrogen bonds between the anion and the pyH^+ cations. All non-hydrogen atoms were refined using anisotropic thermal parameters. The final difference Fourier map was essentially featureless, the largest peak being 0.52 e/Å^3. Final *R* and R_w values are listed in Table 1.

Physical Measurements. Infrared spectra were recorded as Nujol mulls between KBr plates on a Nicolet Model 510P spectrophotometer; solution UV/visible spectra were obtained using a Hewlett-Packard Model 8452A spectrophotometer. Cyclic voltammograms and differential pulse voltammograms were recorded on an IBM EC225

(14) Vincent, J. B.; Chang, H.-R.; Folting, K.; Huffman, J. C.; Christou, G.; Hendrickson, D. N. *J. Am. Chem. Soc.* **1987**, *109*, 5703.

(15) Chisholm, M. H.; Folting, K.; Huffman, J. C.; Kirkpatrick, C. C. *Inorg. Chem.* **1984**, *23*, 1021.

Table 1. Crystallographic Data for $Mn_4O_3X(OAc)_3(dbm)_3$ (X = Cl (**2**) or Br (**3**)) and $(pyH)_3[Mn_4O_3Cl_7(OAc)_3]\cdot 2MeCN$ (**4**)

	2	**3**	**4**
formula	$C_{51}H_{42}O_{15}ClMn_4$	$C_{51}H_{42}O_{15}BrMn_4$	$C_{25}H_{33}N_5O_9Cl_2Mn_4$
fw, g/mol	1150.09	1194.54	1015.48
Space Group	$P2_1/n$	$P2_1/n$	$C2/c$
a, Å	13.900(3)	13.644(2)	37.420(5)
b, Å	22.038(5)	22.190(4)	13.752(1)
c, Å	16.518(5)	16.548(3)	16.139(2)
β, deg	107.80(1)	106.64(1)	110.33(1)
V, Å^3	4816.6	4800.3	7787.9
Z	4	4	8
T, °C	−155	−155	−157
radiation, Mo Kα[a]	0.710 69	0.710 69	0.710 69
ρ_{calc}, g/cm^3	1.586	1.653	1.727
μ, cm^{-1}	11.075	18.801	17.540
octants	$+h,+k,\pm l$	$+h,+k,\pm l$	$+h,+k,\pm l$
no. of unique Data	6,317	6,295	5,105
no. of obsd. Data	2267[b]	2809[b]	2612[c]
$R(R_w)$[d,e]	0.0785 (0.0738)	0.0737 (0.0689)	0.0574 (0.0578)

[a] Graphite monochromator. [b] $F > 2.33\sigma(F)$. [c] $F > 3.0\sigma(F)$. [d] $R = \sum||F_o| - |F_c||/\sum|F_o|$ [e] $R_w = [\sum w(|F_o| - |F_c|)^2/\sum w|F_o|^2]^{1/2}$, where $w = 1/\sigma^2(|F_o|)$.

voltammetric analyzer, a PAR Model 175 Universal Programmer, and a standard three-electrode assembly (a glassy carbon working electrode, a platinum wire auxiliary electrode, and a SCE reference). Tetra-*n*-butylammonium hexafluorophosphate was employed as the supporting electrolyte. Ferrocene under identical conditions was used as an external standard. ^{1}H NMR spectroscopy was performed using a Varian XL-300 spectrometer; chemical shifts are quoted using the δ scale (shifts downfield are positive). Variable-temperature magnetic susceptibility data were obtained with a Series 800 VTS-50 SQUID susceptometer (S.H.E. Corp.) operating at an applied magnetic field strength of 10 kG. Diamagnetic corrections were estimated from Pascal's constants and subtracted from the experimental data to give the molar paramagnetic susceptibilities. The program GENSPIN[16] was used to analyze variable-field magnetization data; the spin of the ground state is set at some quantized value and then the spin Hamiltonian matrix is diagonalized at each magnetic field to least-squares fit the experimental data.

Results

Syntheses. Previous examples of $[Mn_4O_3Cl]^{6+}$-containing complexes ($3Mn^{III},Mn^{IV}$) were obtained by disproportionation reactions of $[Mn^{III}{}_3O]^{7+}$-containing starting materials triggered by carboxylate abstraction with Me_3SiCl.[10] Thus, treatment of $[Mn_3O(OAc)_6(py)_3](ClO_4)$ with Me_3SiCl leads to formation of $Mn_4O_3Cl_4(OAc)_3(py)_3$ (**6**) in >80% yield based on available $MeCO_2^-$. A similar disproportionation reaction but with **1** provided one route to **2** (*vide infra*); the latter was first obtained, however, from a reaction of **1** in CH_2Cl_2 with just 1 equiv of $NBu^n{}_4Cl$. This led to slow crystallization of small amounts (<10% yield based on dbm) of pure **2** in a form suitable for crystallography. Complex **1** is stable in CH_2Cl_2 in the absence of Cl^-. Interestingly, previous work had shown that treatment of **1** in CH_2Cl_2 with NEt_4Cl followed by addition of Et_2O leads to good yields (55−60%) of $(NEt_4)[Mn_7O_4(OAc)_{10}(dbm)_4]$,[17] emphasizing the complexity of the reaction of **1** with Cl^- and rationalizing the low yield of **2** in the present work.

With complex **2** identified, higher yield routes were sought. Complex **1** is stable in hot MeCN (its recrystallization medium) but the addition of 1 equiv of $NBu^n{}_4Cl$ leads on cooling to improved yields (35−43%) of **2**. Even higher yields were obtained when Me_3SiCl was used in place of $NBu^n{}_4Cl$: a ratio dependence study showed that an optimum yield of ∼88% resulted from a **1**:Me_3SiCl ratio of 1:1.5; the yield dropped to 52% for a 1:0.8 ratio, and to 83% (1:3), 73 (1:4), 52 (1:5), and 41% (1:6) as more Me_3SiCl was used. Repetition of the 1:4 reaction with added dbmH did not improve the yield. The formation of **2** via a disproportionation reaction is supported by the coprecipitation of an off-white byproduct which, on the basis of analyses of such solids in analogous past reactions,[10] is the Mn^{II} product of the disproportionation; the latter is readily removed by washing with EtOH.

Using the above observations, eq 1 can be presented as a summary of the reaction; a simplified form of eq 1 that

$$3[Mn_4O_2(O_2CMe)_6(py)_2(dbm)_2] + 2Me_3SiCl \rightarrow 2[Mn_4O_3Cl(O_2CMe)_3(dbm)_3] + 2Me_3SiO_2CMe + 6py + 10MeCO_2^- + 2Mn^{2+} + 2Mn^{3+} \quad (1)$$

$$3[Mn_4O_2]^{8+} + 2Cl^- \rightarrow 2[Mn_4O_3Cl]^{6+} + 2Mn^{2+} + 2Mn^{3+} \quad (2)$$

emphasizes the redox changes is given in eq 2. When $Mn_4O_2(O_2CPh)_6(py)(dbm)_2$ and $Mn_4O_2(O_2CPh)_6(THF)_2(dbm)_2$ instead of **1** were treated with 1.5 equiv of Me_3SiCl in CH_2Cl_2, $Mn_4O_3Cl(O_2CPh)_3(dbm)_3$ was *not* obtained; only starting material was recovered. This suggests that the basicity of the carboxylate is yet another factor important to this reaction, with the more basic AcO^- appearing to favor the disproportionation and formation of a higher oxidation state product.

Analogous reactions with Br^- sources were explored as potential routes to **3**. It should be pointed out that there are very few known examples of stable $Mn^{III}-Br$ bonds owing to redox instability,[18] and *none* with Br^- in a system containing Mn^{IV}. It was thus uncertain whether **3** would be capable of existence. Treatment of **1** with 1 equiv of $NBu^n{}_4Br$ in hot MeCN led to precipitation of a microcrystalline solid whose IR spectrum was almost identical to that of **2** and which therefore appeared to be **3**. However, elemental analysis gave a low Br content and a significant Cl content, the latter presumably a contaminant of the $NBu^n{}_4Br$. Rather than seek to purify the latter, we resorted to the reaction of **1** with Me_3SiBr in CH_2Cl_2; this also led to a nicely crystalline product but

(16) Schmitt, E. A.; Hendrickson, D. N., unpublished results.
(17) Wang, S.; Tsai, H.-L.; Streib, W. E.; Christou, G.; Hendrickson, D. N. *J. Chem. Soc., Chem. Commun.* **1992**, 677.
(18) (a) Morris, R. J.; Girolami, G. S. *Organometallics* **1987**, *6*, 1815. (b) Daugherty, P. A.; Glerup, J.; Goodson, P. A.; Hodgson, D. J.; Michelsen, K. *Acta Chem. Scand.* **1991**, *45*, 244. (c) Bryan, P. S.; Dabrowiak, J. C. *Inorg. Chem.* **1975**, *14*, 297. (d) Goldberg, D. P.; Caneschi, A.; Delfs, C. D.; Sessoli, R.; Lippard, S. J. *J. Am. Chem. Soc.* **1995**, *117*, 5789.

elemental analysis again indicated the presence of both Br and Cl. Finally, the reaction of **1** with Me_3SiBr in CH_2Br_2 gave highly crystalline complex **3** with the expected IR spectrum, a correct Br analysis, and no Cl content. These observations suggest that the Mn_4O_3 unit has a much greater affinity for Cl^- than for Br^-, even to the point that Cl abstraction from CH_2Cl_2 occurs. On the other hand, the successful attainment of **3** confirms that this desired complex can indeed exist and be stable under normal conditions. Attempts to isolate F^--containing products from reactions of **1** with NBu^n_4F proved unsuccessful; reactions with Me_3SiF have not been attempted owing to the strong Si−F bond.

It should be emphasized that eqs 1 and 2 are similar to those previously developed to describe the formation of $Mn_4O_3Cl_4(OAc)_3(py)_3$ (**6**) from the treatment of $[Mn_3O(OAc)_6(py)_3](ClO_4)$ with Me_3SiCl (eq 3).[10] This previous work convinced us that the yield of **6** was now acetate/oxide-limited, as implied in eq 3. We subsequently wondered whether addition of H_2O and

$$3[Mn_3O]^{7+} + Cl^- \rightarrow [Mn_4O_3Cl]^{6+} + 4Mn^{3+} + Mn^{2+} \quad (3)$$

acetic acid to the reaction mixture *after* $[Mn_3O(OAc)_6(py)_3](ClO_4)$ had been treated with Me_3SiCl to trigger disproportionation (and generation of **6**) but *before* crystals of product complex **6** had begun to form might increase the yield of **6** by providing O^{2-} and AcO^- sources. Interestingly, this procedure did indeed increase the yield of product, but the latter was **4**, not complex **6**, i.e., the py groups had been protonated and were present as cations rather than bound to Mn^{III} ions as in **6**. Nevertheless, the added H_2O and acetic acid undoubtedly increase the yield of $[Mn_4O_3Cl]^{6+}$ product by providing O^{2-} and AcO^-, and on this basis the obtained yield of **4** is 75% calculated on available Mn and the disproportionation reaction of eq 4, which indicates

$$5Mn^{III}_3 \rightarrow 3[Mn^{III}_3Mn^{IV}] + 3Mn^{II} \quad (4)$$

a maximum yield of **4** of 80% based on available Mn; i.e., the yield of **4** is essentially quantitative (∼94%). It is paradoxical to note that this high-yield formation of **4** involves adding a water-sensitive carboxylate-abstraction reagent (Me_3SiCl) to $[Mn_3O(OAc)_6(py)_3](ClO_4)$, followed by addition of carboxylate and water back into the reaction mixture.

It should be noted that a number of other tetranuclear Mn complexes with a cubane or distorted-cubane geometry are known, with the vast majority of these being at the Mn^I_4 or Mn^{II}_4 oxidation levels and containing Mn_4X_4 ($X = OH^-, OR^-$, and/or F^-),[19a−e] i.e., not O^{2-}-bridged. Recently, however, a complex with the $[Mn_4O_2(OR)_2]^{4+}$ (i.e., $2Mn^{II}$, $2Mn^{III}$) has been reported and it contains both O^{2-} and phenoxide-like RO^- bridges in the core.[19f]

Description of Structures. Selected interatomic distances and angles for **2**−**4** are collected in Tables 2−4; various ORTEP representations are presented in Figures 1−4. The structures of **2** and **3** (Figures 1 and 2) are isomorphous, and the same atom labeling scheme has been used for both. The asymmetric unit contains only the entire tetranuclear molecule, and the crystallographic symmetry is thus C_1, although the virtual symmetry is C_{3v} with the pseudo-C_3 axis passing through Mn(4) and X(8). The structure consists of a trigonal pyramid of Mn atoms with the μ_3-O^{2-} ion bridging each of the vertical faces and a μ_3-X^- ion bridging the basal face to give a tetra-face-capped trigonal pyramid that may be described for convenience as a highly distorted $[Mn_4O_3X]^{6+}$ cubane unit. Peripheral ligation is provided by three chelating dbm^- and three *syn,syn*-bridging AcO^- groups. Charge considerations indicate a $3Mn^{III},Mn^{IV}$ metal oxidation-state description, and metric parameters indicate that apical Mn(4) is the Mn^{IV} center. The $3Mn^{III}$ atoms, Mn(2)−Mn(4), are Jahn−Teller (JT) distorted (elongated) as expected for a high-spin d^4 ion in near-octahedral geometry, and the JT axes are the ones that include the Mn^{III}−X bonds. The structures of the cores of **2** and **3** are thus similar to those previously reported for other $[Mn_4O_3Cl]^{6+}$-containing complexes.[10,11] The disposition of the three dbm^- groups in **2** and **3** places their six Ph rings in a skirtlike fashion around the basal Mn^{III}_3 face of the trigonal pyramid, and this gives a concave cavity inside which is situated the μ_3-X^- ion. This is shown for **2** as a space-filling stereoview in Figure 3, viewed approximately along the virtual C_3 axis.

Table 2. Comparison of Selected Interatomic Distances (Å) for $Mn_4O_3X(OAc)_3(dbm)_3$ (X = Cl (**2**) or Br (**3**))

	2	**3**		**2**	**3**
Mn1···Mn2	2.797(5)	2.804(4)	Mn1···Mn3	2.797(4)	2.786(3)
Mn1···Mn4	2.792(5)	2.793(4)	Mn2···Mn3	3.252(4)	3.274(3)
Mn2···Mn4	3.237(5)	3.286(4)	Mn3···Mn4	3.264(4)	3.285(4)
Mn1−O5	1.883(15)	1.856(11)	Mn1−O6	1.867(14)	1.871(12)
Mn1−O7	1.842(13)	1.857(12	Mn1−O9	1.962(14)	1.958(12)
Mn1−O13	1.903(14)	1.918(11)	Mn1−O19	1.930(14)	1.926(13)
Mn2−X8	2.641(7)	2.802(3)	Mn2−O5	1.926(14)	1.918(13)
Mn3−X8	2.656(7)	2.807(3)	Mn2−O11	2.139(14)	2.168(13)
Mn4−X8	2.654(7)	2.799(3)	Mn2−O25	1.921(15)	1.915(12)
Mn2−O7	1.945(14)	1.950(12)	Mn3−O5	1.922(15)	1.915(12)
Mn2−O21	1.911(14)	1.878(14)	Mn3−O17	2.186(13)	2.174(12)
Mn3−O6	1.945(13)	1.947(12)	Mn3−O42	1.927(14)	1.930(12)
Mn3−O38	1.902(15)	1.927(12)	Mn4−O6	1.920(13)	1.937(12)
Mn4−O7	1.939(14)	1.915(11)	Mn4−O15	2.170(14)	2.148(12)
Mn4−O55	1.916(14)	1.930(13)	Mn4−O59	1.893(14)	1.905(14)

The structural parameters for **2** and **3** are listed in Tables 2 and 3 in a manner that allows ready comparison. Examination of these tables emphasizes that the two structures are essentially congruent except for the halide region of the molecules. Thus, almost all interatomic distances and angles are within the 6σ criterion except the following: the Mn−Cl distances in **2** (2.641(7)−2.656(7) Å) are significantly shorter than the Mn−Br distances in **3** (2.799(3)−2.807(3) Å); the difference (0.15−0.16 Å) is comparable with the difference in ionic radii (0.12 Å) for six-coordinate X^-);[20a] (ii) the Mn−Cl−Mn angles (75.37(19)−75.85(19)°) are larger than Mn−Br−Mn angles (71.43(9)−71.83(9)°), consistent with the longer Mn−Br bonds; and (iii) $Mn^{III}\cdots Mn^{III}$ separations increase *very* slightly in going from **2** to **3** (3.237(5)−3.264(4) Å vs 3.274(3)−3.286(4) Å), individual changes being at the borderline of statistical significance but appearing to be real. Note, in contrast, that the $Mn^{III}\cdots Mn^{IV}$ distances are identical in the two structures.

Complex **4** contains a $[Mn_4(\mu_3\text{-}O)_3(\mu_3\text{-}Cl)]^{6+}$ core essentially identical to that in **2**, and with μ-AcO^- groups bridging each $Mn^{III}\cdots Mn^{IV}$ pair (Figure 4). However, the other peripheral ligands on the Mn^{III} atoms are now all terminally coordinated Cl^- ions giving a $[Mn_4O_3Cl_7(OAc)_3]^{3-}$ trianion. As for **2** and **3**, there is no crystallographically imposed symmetry in **4**, but the anion has virtual C_{3v} symmetry. The cations are three pyridinium (pyH^+) groups whose protonated nature is clearly evidenced by their participation in hydrogen-bonding interac-

(19) (a) Horn, E.; Snow, M. R.; Zeleny, P. C. *Aust. J. Chem.* **1980**, *33*, 1659. (b) Abel, E. W.; Towle, I. D. H.; Cameron, T. S.; Cordes, R. E. *J. Chem. Soc., Dalton Trans.* **1979**, 1943. (c) Brooker, S.; McKee, V.; Shepard, W. B.; Pannell, L. K. *J. Chem. Soc., Dalton Trans.* **1987**, 2555. (d) Smit, J. J.; Nap, G. M.; DeJongh, L. J.; Van Ooijen, J. A. C.; Reedijk, J. *Physica* **1979**, *97B*, 365. (e) Taft, K. L.; Caneschi, A.; Pence, L. E.; Delfs, C. D.; Papaefthymiou, G. G.; Lippard, S. J. *J. Am. Chem. Soc.* **1993**, *115*, 11753. (f) Mikuriya, M.; Hashimoto, Y.; Kawamori, A. *Chem. Lett.* **1995**, 1095.

(20) (a) Shannon, R. D. *Acta Crystallogr. Sect. A* **1976**, *A32*, 751. (b) Kambe, K. *J. Phys. Soc. Jpn.* **1950**, *5*, 48.

Table 3. Comparison of Selected Bond Angles (deg) for $Mn_4O_3X(OAc)_3(dbm)_3$ (X = Cl (**2**) or Br (**3**))

	2	**3**		**2**	**3**
O5−Mn1−O7	85.4(6)	84.3(5)	O5−Mn1−O6	84.9(5)	85.1(5)
O5−Mn1−O13	178.5(6)	178.8(5)	O5−Mn1−O9	95.2(6)	96.0(5)
O6−Mn1−O7	85.2(6)	84.7(5)	O5−Mn1−O19	94.2(6)	94.8(5)
O6−Mn1−O13	93.7(6)	93.8(5)	O6−Mn1−O9	177.0(6)	177.7(5)
O7−Mn1−O9	91.8(6)	93.3(5)	O6−Mn1−O19	93.9(6)	93.1(5)
O7−Mn1−O19	179.1(6)	179.1(5)	O7−Mn1−O13	94.2(6)	95.3(5)
O9−Mn1−O19	89.1(6)	86.8(5)	O9−Mn1−O13	86.2(6)	85.2(5)
X8−Mn2−O5	84.6(5)	85.6(3)	O13−Mn1−O19	86.2(6)	85.6(5)
X8−Mn2−O11	171.9(4)	173.5(4)	X8−Mn2−O7	86.0(4)	85.4(3)
X8−Mn2−O25	93.5(5)	92.7(4)	X8−Mn2−O21	93.7(4)	91.9(4)
O5−Mn2−O11	90.4(6)	91.8(5)	O5−Mn2−O7	81.5(6)	80.2(5)
O5−Mn2−O25	94.7(6)	96.0(5)	O5−Mn2−O21	173.4(6)	172.0(5)
O7−Mn2−O21	92.1(6)	92.1(5)	O7−Mn2−O11	87.0(5)	88.2(5)
O11−Mn2−O21	90.6(6)	89.9(5)	O7−Mn2−O25	176.2(6)	175.8(5)
O21−Mn2−O25	91.7(6)	91.7(5)	O11−Mn2−O25	93.2(6)	93.5(5)
X8−Mn3−O6	84.2(4)	86.0(3)	X8−Mn3−O5	84.2(4)	85.5(4)
X8−Mn3−O38	92.0(5)	90.7(4)	X8−Mn3−O17	171.7(4)	174.0(3)
O5−Mn3−O6	81.8(6)	81.4(4)	X8−Mn3−O42	96.0(5)	93.1(4)
O5−Mn3−O38	90.8(7)	93.2(5)	O5−Mn3−O17	90.2(5)	91.0(5)
O6−Mn3−O17	89.0(5)	88.6(5)	O5−Mn3−O42	177.1(7)	173.7(5)
O6−Mn3−O42	95.4(6)	92.4(5)	O6−Mn3−O38	172.0(6)	173.9(5)
O17−Mn3−O42	89.3(6)	89.8(5)	O17−Mn3−O38	94.2(6)	94.4(5)
X8−Mn4−O6	84.7(4)	86.5(4)	O38−Mn3−O42	92.1(6)	93.0(5)
X8−Mn4−O15	172.2(4)	174.7(4)	X8−Mn4−O7	85.7(4)	86.2(3)
X8−Mn4−O59	96.2(5)	94.4(4)	X8−Mn4−O55	89.8(4)	90.1(4)
O6−Mn4−O15	88.3(6)	88.9(5)	O6−Mn4−O7	81.2(5)	81.4(5)
O6−Mn4−O59	172.6(7)	173.2(5)	O6−Mn4−O55	94.4(6)	94.1(5)
O7−Mn4−O55	174.0(5)	174.3(5)	O7−Mn4−O15	89.6(5)	90.7(5)
O15−Mn4−O55	94.4(6)	92.7(5)	O7−Mn4−O59	91.5(6)	91.9(5)
O55−Mn4−O59	93.0(6)	92.7(5)	O15−Mn4−O59	90.3(6)	89.9(5)
Mn2−X8−Mn4	75.37(19)	71.83(9)	Mn2−X8−Mn3	75.74(19)	71.43(9)
Mn1−O5−Mn2	94.5(7)	96.0(6)	Mn3−X8−Mn4	75.85(19)	71.74(10)
Mn2−O5−Mn3	115.4(7)	117.4(6)	Mn1−O5−Mn3	94.6(6)	95.3(5)
Mn1−O6−Mn4	95.0(6)	94.3(5)	Mn1−O6−Mn3	94.4(6)	93.7(6)
Mn1−O7−Mn2	95.2(6)	94.9(5)	Mn3−O6−Mn4	115.2(7)	115.5(6)
Mn2−O7−Mn4	112.9(6)	116.4(5)	Mn1−O7−Mn4	95.2(6)	95.5(5)

tions with the anion (Figure 4). Interestingly, the pyH^+ groups interact with the anion in two different ways: the pyH^+ group containing N(27) has its N−H vector pointing approximately to the midpoint between Cl(7) and Cl(8), with resultant N(27)···Cl(7) and N(27)···Cl(8) distances of 3.401 and 3.344 Å, respectively, indicating a N−H···2 Cl three-center hydrogen-bonding situation; the pyH^+ group containing N(33) is similar (although a little more asymmetric), with N(33)···Cl(9) and N(33)···Cl(10) distances of 3.687 and 3.150 Å, respectively. In contrast, the third pyH^+ group containing N(39) is oriented differently to the other two and has its N−H vector pointing approximately to the midpoint of the Cl(6), Cl(11), and O(14) face, with distances of N(39) from these three atoms of 3.453, 3.522, and 2.855 Å, respectively. In fact, the N(27)···O(12) and N(33)···O(13) distances are 2.866 and 2.970 Å, respectively, and although the N−H−O angles would be rather acute, it is likely that weak N−H···O interactions are present at these two pyH^+ groups also, rationalizing why all three pyH^+ groups are so compactly organized about the $[Mn_4O_3Cl]$ core rather than projecting outward or above the plane of six terminal Cl^- ions.

Magnetic Susceptibility Studies. Variable-temperature, solid-state magnetic susceptibility studies were performed on powdered samples of complexes **2**−**4** in an applied magnetic field of 10.0 kG and in the temperature ranges of 5.01−300.0 and 5.01−320.0 K, respectively. Plots of effective magnetic moment (μ_{eff}) per molecule vs temperature are presented in Figures 5−7, and they can be seen to be similar for the three complexes. For **2**, μ_{eff} steadily increases from 8.95 μ_B at 300 K to a plateau value of 9.88 μ_B at 30.0 K and then decreases sharply below ∼12 K to 9.36 μ_B at 5.01 K. For **3**, μ_{eff} increases from 9.06 μ_B at 320 K to 10.13 μ_B at 30.0 K and then decreases sharply below ∼12 K to 9.54 μ_B at 5.01 K. For **4**, μ_{eff} increases from 8.87 μ_B at 320.0 K to 9.95 μ_B at 11.0 K, whereupon there is a decrease to 9.61 μ_B at 5.01 K. These data are plotted in Figure 7.

If there were no exchange interactions between the metal ions in a $Mn^{III}_3Mn^{IV}$ complex, the spin-only ($g = 2$) μ_{eff} value would be 9.33 μ_B and it would be temperature independent. The metal ions are thus clearly involved in magnetic exchange interactions, and the data were therefore fit to the theoretical expression derived previously[10] for the χ_M vs T behavior of a $Mn^{III}_3Mn^{IV}$ trigonal pyramid of C_{3v} symmetry. This expression was derived from the spin Hamiltonian of eq 5, where $J = J(Mn^{III}\cdots Mn^{IV})$,

$$\hat{H} = -2J(S_1\cdot S_2 + S_1\cdot S_3 + S_2\cdot S_3) - 2J'(S_2\cdot S_3 + S_2\cdot S_4 + S_3\cdot S_4) \quad (5)$$

$J' = J(Mn^{III}\cdots Mn^{III})$, $S_1 = S(Mn^{IV}) = {}^3/_2$ and $S_2 = S_3 = S_4 = S(Mn^{III}) = 2$, by employing an equivalent operator approach based on the Kambe vector coupling method.[20b] As described in detail elsewhere,[10] this leads to the eigenvalue expression of eq 6, which gives the energy, $E(S_T)$, of each of the possible

$$E(S_T) = -J[S_T(S_T + 1) - S_A(S_A + 1)] - J'[S_A(S_A + 1)] \quad (6)$$

total spin states, S_T, of the $Mn^{III}_3Mn^{IV}$ complex, where $\hat{S}_A = \hat{S}_2 + \hat{S}_3 + \hat{S}_4$ and $\hat{S}_T = \hat{S}_1 + \hat{S}_A$.

The fits of the experimental χ_M vs T data to the theoretical expression are shown as solid lines in Figures 5−7: the fitting parameters for **2** are $J = -28.4$ cm^{-1}, $J' = +8.3$ cm^{-1}, and $g = 1.98$; those for **3** are $J = -30.1$ cm^{-1}, $J' = +7.4$ cm^{-1}, and $g = 2.03$; and those for **4** are $J = -29.1$ cm^{-1}, $J' = +10.2$ cm^{-1}, and $g = 1.97$. These values yield an $S = {}^9/_2$ ground

Table 4. Selected Bond Distances and Angles for $(pyH)_3[Mn_4O_3Cl_7(OAc)_3]\cdot 2MeCN$ (**4**)

Mn(1)···Mn(4)	2.838(2)	Mn(2)-O(12)	1.973(9)
Mn(2)···Mn(4)	2.817(3)	Mn(2)−O(13)	1.936(9)
Mn(3)···Mn(4)	2.832(3)	Mn(2)−O(19)	2.152(10)
Mn(1)−Cl(5)	2.652(3)	Mn(3)−Cl(5)	2.657(4)
Mn(1)−Cl(6)	2.249(4)	Mn(3)−Cl(10)	2.281(4)
Mn(1)−Cl(7)	2.273(4)	Mn(3)−Cl(11)	2.255(4)
Mn(1)−O(12)	1.961(9)	Mn(3)−O(13)	1.969(9)
Mn(1)−O(14)	1.980(9)	Mn(3)−O(14)	1.925(9)
Mn(1)−O(15)	2.165(9)	Mn(3)−O(23)	2.187(10)
Mn(1)···Mn(2)	3.306(3)	Mn(4)−O(12)	1.855(9)
Mn(2)···Mn(3)	3.293(3)	Mn(4)−O(13)	1.872(9)
Mn(1)···Mn(3)	3.307(3)	Mn(4)−O(14)	1.869(9)
Mn(2)−Cl(5)	2.592(4)	Mn(4)−O(17)	1.969(10)
Mn(2)−Cl(8)	2.271(4)	Mn(4)−O(21)	1.941(9)
Mn(2)−Cl(9)	2.270(4)	Mn(4)−O(25)	1.942(10)

Cl(5)−Mn(1)−Cl(6)	95.10(13)	Cl(6)−Mn(1)−O(12)	172.9(3)	Cl(10)−Mn(3)−Cl(11)	94.32(16)	O(12)−Mn(4)−O(17)	95.7(4)
Cl(5)−Mn(1)−Cl(7)	97.05(12)	Cl(6)−Mn(1)−O(14)	93.41(28)	Cl(10)−Mn(3)−O(13)	92.9(3)	O(12)−Mn(4)−O(21)	93.4(4)
Cl(5)−Mn(1)−O(12)	83.0(3)	Cl(6)−Mn(1)−O(15)	91.6(3)	Cl(10)−Mn(3)−O(14)	172.9(3)	O(12)−Mn(4)−O(25)	178.6(4)
Cl(5)−Mn(1)−O(14)	83.14(28)	Cl(7)−Mn(1)−O(12)	92.23(28)	Cl(10)−Mn(3)−O(23)	88.2(3)	O(13)−Mn(4)−O(14)	84.3(4)
Cl(5)−Mn(1)−O(15)	168.42(27)	Cl(7)−Mn(1)−O(14)	171.77(27)	Cl(11)−Mn(3)−O(13)	172.1(3)	O(13)−Mn(4)−O(17)	176.5(4)
Cl(6)−Mn(1)−Cl(7)	94.76(14)	Cl(7)−Mn(1)−O(15)	91.76(27)	Cl(11)−Mn(3)−O(14)	92.6(3)	O(13)−Mn(4)−O(21)	95.5(4)
O(12)−Mn(1)−O(14)	79.6(4)	Cl(8)−Mn(2)−O(13)	173.5(3)	Cl(11)−Mn(3)−O(23)	96.0(3)	O(13)−Mn(4)−O(25)	92.4(4)
O(12)−Mn(1)−O(15)	89.1(4)	Cl(8)−Mn(2)−O(19)	91.8(3)	O(13)−Mn(3)−O(14)	80.3(4)	O(14)−Mn(4)−O(17)	92.5(4)
O(14)−Mn(1)−O(15)	87.1(4)	Cl(9)−Mn(2)−O(12)	172.6(3)	O(13)−Mn(3)−O(23)	87.4(4)	O(14)−Mn(4)−O(21)	178.7(4)
Cl(5)−Mn(2)−Cl(8)	94.27(15)	Cl(9)−Mn(2)−O(13)	92.0(3)	O(14)−Mn(4)−O(25)	95.4(4)	Mn(2)−O(12)−Mn(4)	94.7(4)
Cl(5)−Mn(2)−Cl(9)	95.53(15)	Cl(9)−Mn(2)−O(19)	91.1(3)	O(17)−Mn(4)−O(21)	87.8(4)	Mn(2)−O(13)−Mn(3)	115.0(4)
Cl(5)−Mn(2)−O(12)	84.4(3)	O(12)−Mn(2)−O(13)	80.6(4)	O(17)−Mn(4)−O(25)	85.5(4)	Mn(2)−O(13)−Mn(4)	95.4(4)
Cl(5)−Mn(2)−O(13)	84.83(27)	O(12)−Mn(2)−O(19)	88.1(4)	O(21)−Mn(4)−O(25)	86.0(4)	Mn(3)−O(13)−Mn(4)	95.0(4)
Cl(5)−Mn(2)−O(19)	170.6(3)	O(13)−Mn(2)−O(19)	88.3(4)	Mn(1)−Cl(5)−Mn(2)	78.14(10)	Mn(1)−O(14)−Mn(3)	115.8(5)
Cl(8)−Mn(2)−Cl(9)	94.57(16)	Cl(5)−Mn(3)−Cl(10)	97.25(15)	Mn(1)−Cl(5)−Mn(3)	77.05(10)	Mn(1)−O(14)−Mn(4)	95.0(4)
Cl(8)−Mn(2)−O(12)	92.9(3)	Cl(5)−Mn(3)−Cl(11)	93.51(16)	Mn(2)−Cl(5)−Mn(3)	77.70(11)	Mn(3)−O(14)−Mn(4)	96.5(4)
Cl(5)−Mn(3)−O(13)	82.47(27)	O(14)−Mn(3)−O(23)	89.4(4)	Mn(1)−O(12)−Mn(2)	114.4(5)		
Cl(5)−Mn(3)−O(14)	84.0(3)	O(12)−Mn(4)−O(13)	85.5(4)	Mn(1)−O(12)−Mn(4)	96.1(4)		
Cl(5)−Mn(3)−O(23)	168.7(3)	O(12)−Mn(4)−O(14)	85.3(4)				

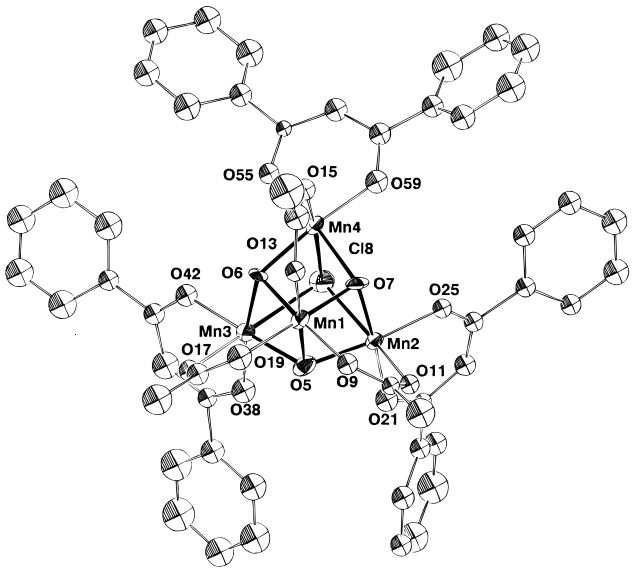

Figure 1. ORTEP representation of **2** at the 50% probability level.

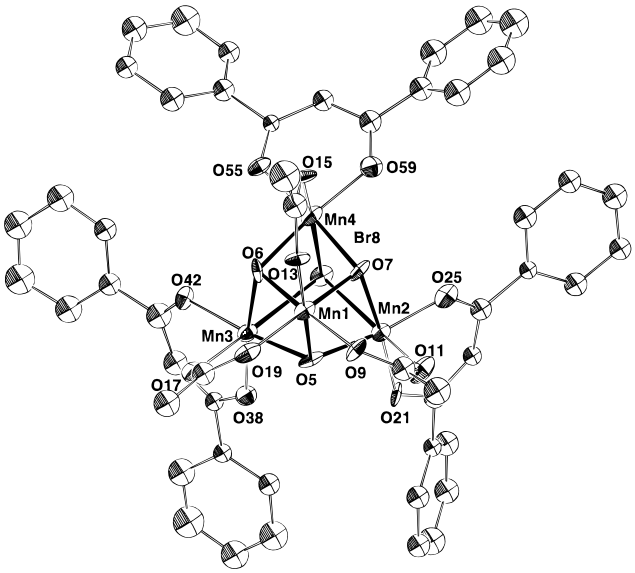

Figure 2. ORTEP representation of **3** at the 50% probability level.

state for all three complexes, with $S = {}^7/_2$ and $S = {}^{11}/_2$ first and second excited states, respectively. Only data for temperatures ≥30 K were employed in the fits because below this temperature the effects of zero-field splitting (ZFS) become significant and result in the rapid decrease in μ_{eff} values.

In order to confirm the spin of the ground state and to determine the magnitude of the ZFS parameter *D*, magnetization (*M*) vs magnetic field (*H*) studies were performed on complexes **2** and **3** at 5.0 (2−4 K), 10.0 (2−30 K), 20.0 (2−4 K), 30.0 (2−4 K), 40.0 (2−4 K), and 50.0 kG (2−30 K). The data are plotted in Figures 8 and 9 as reduced magnetization ($M/N\mu_B$) vs H/T. In the absence of ZFS and at temperatures where only the ground state is populated, the $M/N\mu_B$ vs H/T plots would follow the Brillouin function, which has a maximum value of $M/N\mu_B$ of gS_T (i.e., a value of 9 for $S_T = {}^9/_2$ and $g = 2$) at low temperatures and high fields, and the various isofield lines would be superimposed. As can be seen in Figures 8 and 9, the maximum $M/N\mu_B$ values for **2** and **3** are 8.56 for **2** and 8.51 for **3**, values consistent with an $S_T = {}^9/_2$ ground state, and the six isofield lines do not superimpose; the latter deviations from the Brillouin function result from ZFS within the $S_T = {}^9/_2$ ground state.

The $M/N\mu_B$ vs H/T data for **2** and **3** were least-squares fit. For each setting of the parameters *g* and *D*, the spin Hamiltonian matrix was diagonalized. For both complexes, the best fit of the data was found by assuming an isolated ground state with

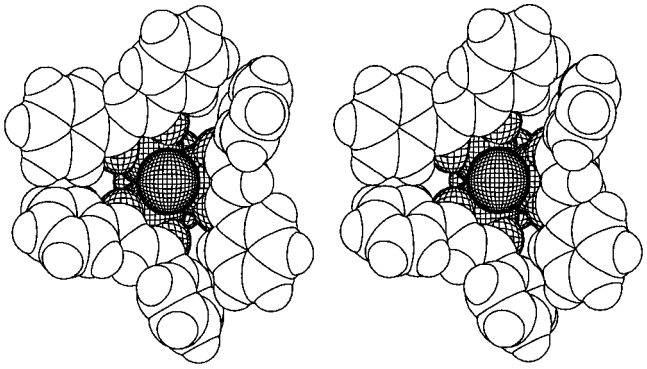

Figure 3. Space-filling stereoview of **2**, viewed approximately along the $Mn^{IV}\cdots Cl$ vector, emphasizing the location of the Cl in a cavity formed by the three dbm groups.

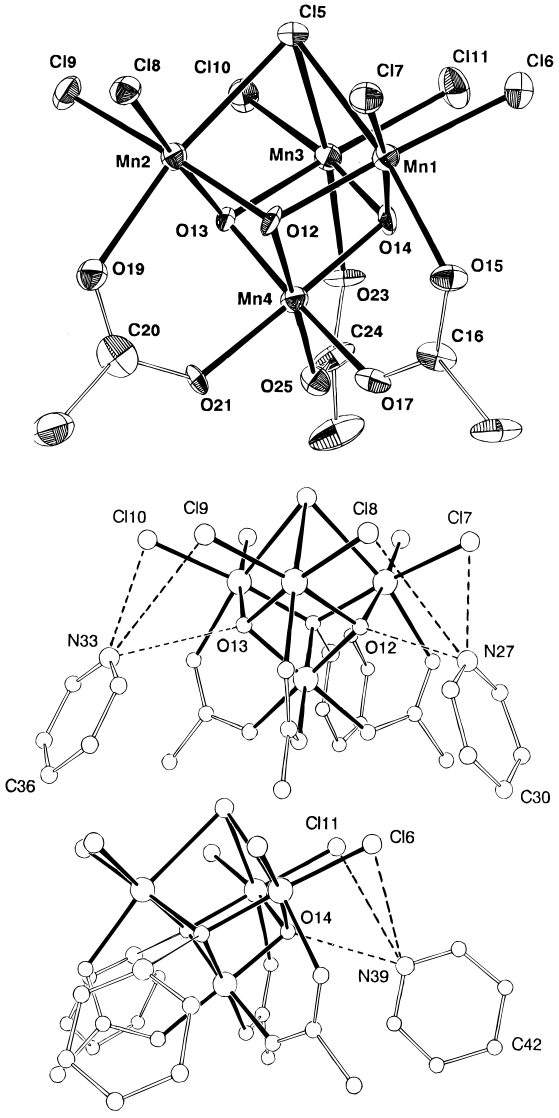

Figure 4. ORTEP representation of the $[Mn_4O_3Cl_7(O_2CMe)_3]^{3-}$ anion of **4** (top) and views showing the hydrogen-bonding interactions between the anion and pyH^+ cations (center and bottom).

$S = {}^9/_2$. In the case of **2**, the data could be fit with $D = +0.55$ cm^{-1} and $g = 2.03$; the solid lines in Figure 8 show that this fit is good. An equally good fit could be obtained with $D < 0$ with the values $D = -0.40$ cm^{-1} and $g = 2.00$. For complex **3**, the data were fit to give $D = 0.55$ cm^{-1} and $g = 2.02$ (solid lines in Figure 9); these data were equally accommodated by $D = -0.35$ cm^{-1} and $g = 1.99$. It is well-known that in fitting variable-field magnetization data for a polycrystalline

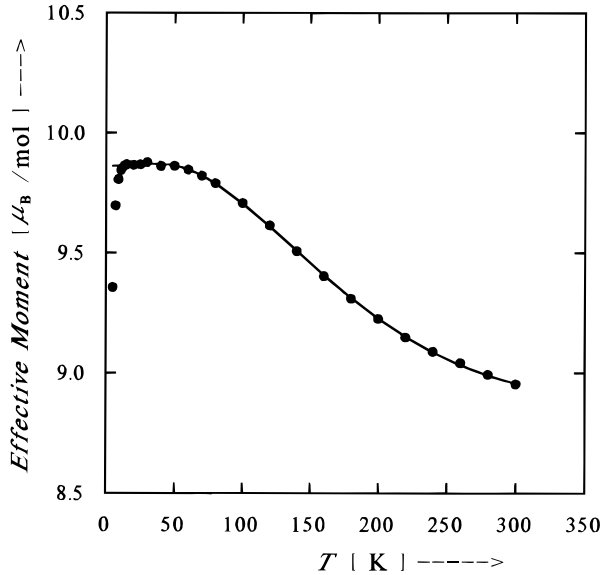

Figure 5. Effective magnetic moment, μ_{eff}, vs temperature for **2**. The solid line is a fit of the experimental data to the theoretical expression; see the text for the fitting parameters.

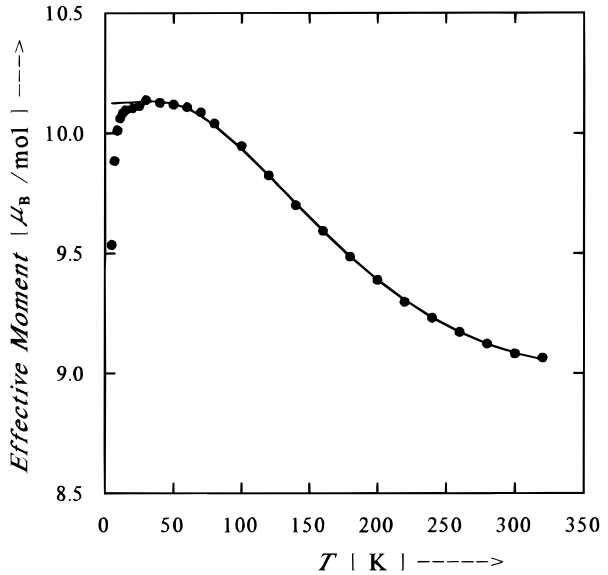

Figure 6. Effective magnetic moment, μ_{eff}, vs temperature for **3**. The solid line is a fit of the experimental data to the theoretical expression; see the text for the fitting parameters.

sample, minima can be found for both $D > 0$ and $D < 0$. In the present case, $D<0$ is likely the true situation, since D values for mononuclear, octahedral, JT elongated Mn^{III} ions are negative,[21] the three Mn^{III} ions in the $[Mn_4O_3X]^{6+}$ core are all JT elongated, and the D value for the ground state of the tetranuclear complexes is a vectorial coupling of the D values for the three Mn^{III} ions. A $D < 0$ situation for the $[Mn_4O_3X]^{6+}$ core is also suggested by the results of AC susceptibility studies.[21]

The values of J, J', g, and D obtained for **2** and **3** from the above studies may be compared with those obtained for previous examples of $[Mn_4O_3Cl]^{6+}$-containing complexes with pyridine (or imidazole) and Cl^- as terminal ligands in place of the dbm^- groups.[10,11] These data are collected in Table 5, which also provides information on the first and second excited states. As can be seen, all $[Mn_4O_3X]^{6+}$-containing complexes prepared

(21) Aubin, S. M. J.; Wemple, M. W.; Adams, D. M.; Tsai, H.-L.; Christou, G.; Hendrickson, D. N. *J. Am. Chem. Soc.* **1996**, *118*, 7746.

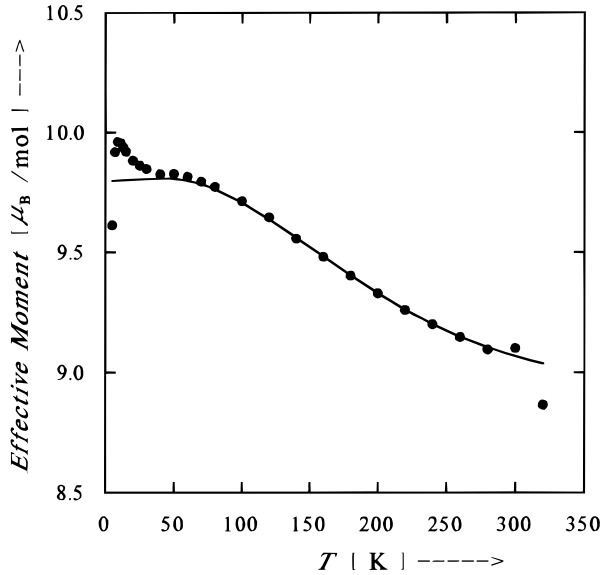

Figure 7. Effective magnetic moment, μ_{eff}, vs temperature for **4**. The solid line is a fit of the experimental data to the theoretical expression; see the text for the fitting parameters. The increase in μ_{eff} at temperatures $\leq$30 K is due to torquing of the microcrystallites in the applied magnetic field.

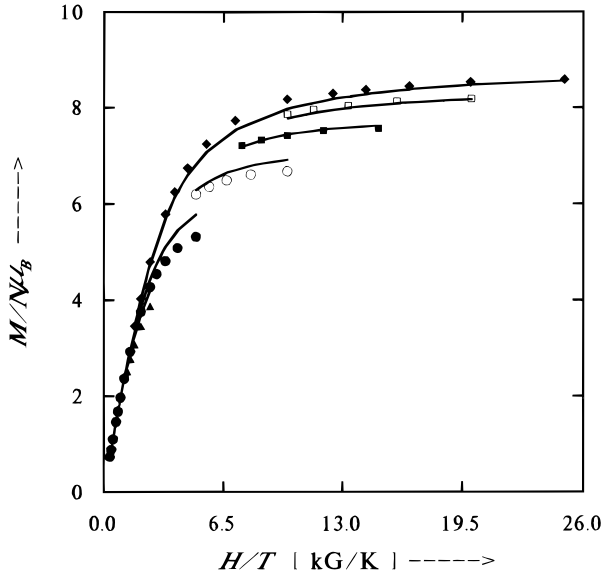

Figure 8. Reduced magnetization, $M/N\mu_B$ vs H/T for **2**. Data were collected at (▲) 50.0, (□) 40.0, (■) 30.0, (○) 20.0, (●) 10.0, and (▲) 5.0 kG. The solid lines result from a least-squares fit of the data with diagonalization of the spin Hamiltonian matrix at each setting of the parameters D and g; see text for the values of the parameters.

possess $S_T = {}^9/_2$, ${}^7/_2$, and ${}^{11}/_2$ ground, first excited, and second excited states, respectively. The differences observed between these various complexes are relatively small with the various J, J', and D values being of comparable magnitude. In all cases, the exchange interactions gauged by J and J' are antiferromagnetic and ferromagnetic, respectively, with the former being of greater strength by a factor of 2−4.

^{1}H NMR Spectroscopy. Proton NMR studies on complexes **2** and **3** have been carried out to probe their identity and stability in solution. Owing to the limited solubility of these complexes except in chlorinated hydrocarbons, these studies were performed in $CDCl_3$ solution. The two complexes give essentially superimposable spectra, and only the spectrum for complex **3** is shown in Figure 10; the number of resonances is consistent with effective C_{3v} symmetry in solution and, therefore, retention of the solid-state structure on dissolution in this solvent. The

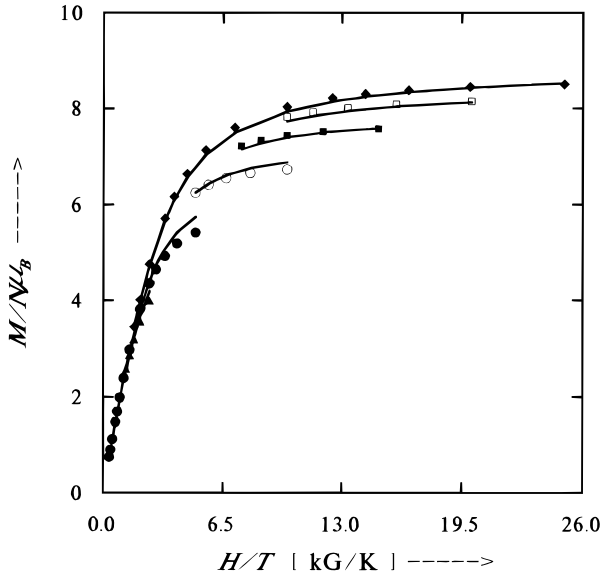

Figure 9. Plots of the reduced magnetization, $M/N\mu_B$ vs H/T for **3**. Data were collected at (◆) 50.0, (□) 40.0, (■) 30.0, (○) 20.0, (●) 10.0, and (▲) 5.0 kG. The solid lines result from a least-squares fit of the data with diagonalization of the spin Hamiltonian matrix at each setting of the parameters D and g; see text for the values of the parameters.

Table 5. Comparison of Fitting Parameters and Low-Lying Electronic States of $[Mn_4O_3X]^{6+}$-Containing Complexes

parameter[a]	**2**	**3**	**4**	**5**	**6**	**7**	**8**
J, cm^{-1}	−28.4	−30.1	−29.1	−30.3	−23.1	−20.8	−27.1
J', cm^{-1}	8.3	7.4	10.2	11.1	11.3	8.6	11.1
g	1.98	2.03	1.97	1.92	1.86	2.00	1.95
ground S_T	${}^9/_2$	${}^9/_2$	${}^9/_2$	${}^9/_2$	${}^9/_2$	${}^9/_2$	${}^9/_2$
$E(S_T = {}^7/_2)$[b]	185	179	210	224	205	165	215
$E(S_T = {}^{11}/_2)$[b]	331	321	320	333	254	229	298
D, cm^{-1}	0.55	0.55	na	0.32	0.28	na[e]	na
ref	*c*	*c*	*c*	*d*	*d*	*d*	*d*

[a] $J = J(Mn^{III}\cdots Mn^{IV})$, $J' = J(Mn^{III}\cdots Mn^{III})$. [b] Versus the $S_T = {}^9/_2$ ground state, which is taken as the zero of energy. [c] This work. [d] References 10 and 11. Complexes: **5** = $(H_2Im)_2[Mn_4O_3Cl_6(OAc)_3(HIm)]$; **6** = $[Mn_4O_3Cl_4(OAc)_3(py)_3]$; **7** = $[Mn_4O_3Cl_4(O_2CEt)_3(py)_3]$; **8** = $[Mn_4O_3Cl_4(O_2CC_6H_3\text{-}m\text{-}Cl_2)_3(py)_3]$. [e] na, not available.

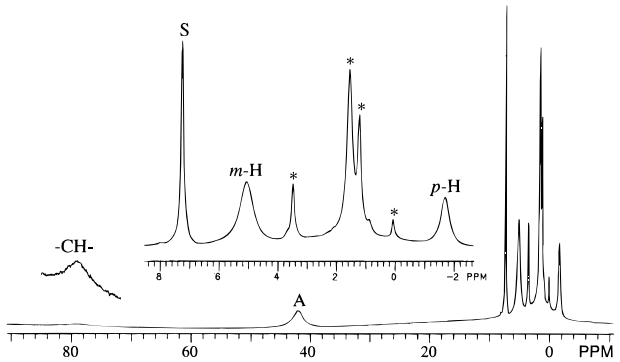

Figure 10. ^{1}H NMR spectrum of **3** in $CDCl_3$ at ∼23 °C showing an expansion of the $\delta = -2$ to +8 ppm region. Peaks due to water, solvate Et_2O molecules and other impurities are marked with an asterisk; the broad resonance at δ ∼79 ppm is the dbm methine hydrogen. A = acetate; S = $CHCl_3$.

chemical shifts are listed in Table 6. The $MeCO_2^-$ resonance at $\delta \approx 42$ ppm is diagnostic for this group attached to the $[Mn_4O_3Cl]^{6+}$ core.[10] The dbm signals were assigned by consideration of relative broadnesses and integration ratios; the dbm methine proton is dramatically broadened and paramagnetically shifted downfield to $\delta \approx 79$ ppm, consistent with its close proximity to the metal centers. Integration of the two signals at $\delta = 5.1$ and $\delta = -1.7$ ppm gave a 2:1 ratio,

Table 6. ^{1}H NMR Data[a] for Complexes **2**−**4**

proton	**2**	**3**	**4**
para H	−1.52	−1.65	
meta H	5.08	5.09	
ortho H	no[b]	no	
$MeCO_2^-$	42.4	42.3	39.0
CH	78.1	79.3	

[a] In $CDCl_3$ (**2**, **3**) or CD_3CN (**4**) solution at −23 °C; quoted numbers are chemical shifts in ppm referenced to TMS using the solvent $CHCl_3$ (δ = 7.26 ppm) or CHD_2CN (δ = 1.94 ppm) signal as an internal standard. [b] no, not observed (obscured by impurities).

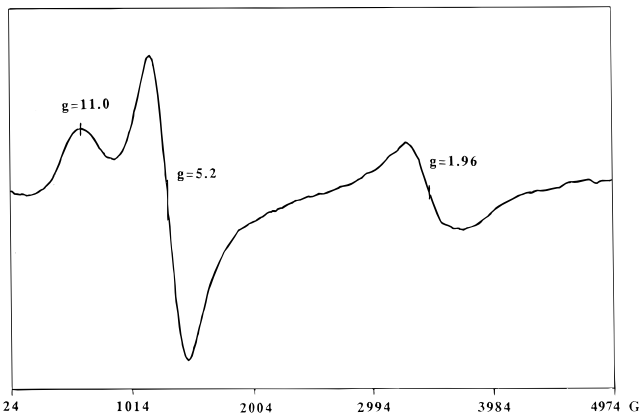

Figure 11. X-band EPR spectrum of **2** in a CH_2Cl_2/toluene (1:1) glass at 5 K.

respectively, indicating the latter signal to be from the dbm *para* hydrogen atoms; the former is assigned to the *meta* hydrogen atoms. The resonance due to the *ortho* hydrogen atoms is not observed in the spectra of **2** or **3** but it is in fact at $\delta \approx 1.5$ ppm and it is thus obscured by the solvent impurity peaks in that region; in other $[Mn_4O_3X]^{6+}$-containing species ($X = N_3^-$, NCO^-, F^-, $MeCO_2^-$, etc.) prepared more recently,[22,23] the δ = 1−2 ppm region is often unobscured, and in those cases the dbm *ortho* hydrogen resonance is observed as a broad signal centered at $\delta \approx 1.5$ ppm.

EPR Spectroscopy. Previous examples of complexes containing the $[Mn_4O_3Cl]^{6+}$ core and possessing an $S_T = {}^9/_2$ ground state have been found to be EPR-active,[10,11] and the same is true for both **2** and **3**. The EPR spectrum of **2** is shown in Figure 11; the spectrum was recorded as a CH_2Cl_2/toluene (1:1) glass at 5 K and shows three main features at *g* values of 11.0, 5.2, and 1.96. The overall profile and measured *g* values are essentially identical to those for **2** and very similar to those for previous $[Mn_4O_3Cl]^{6+}$ species with py/Cl^- in place of dbm^-.

Electrochemistry. Complexes **2** and **3** have been investigated by cyclic voltammetry (CV) and differential pulse voltammetry (DPV). The CV scan for **2** is shown in Figure 12; that for complex **3** looks extremely similar. The CV/DPV traces for **2** and **3** show two reversible features, a one-electron oxidation and a one-electron reduction at DPV peak potentials (in the format **2**/**3**) of 1.09/1.06 and −0.25/−0.21 V; both complexes also show a second, irreversible reduction at much more negative potentials (−1.4 to −1.5 V). These data indicate that substitution of Br^- for Cl^- results in complex **3** becoming slightly easier to reduce *and* easier to oxidize, but the differences are small. For both the reversible oxidation and reduction

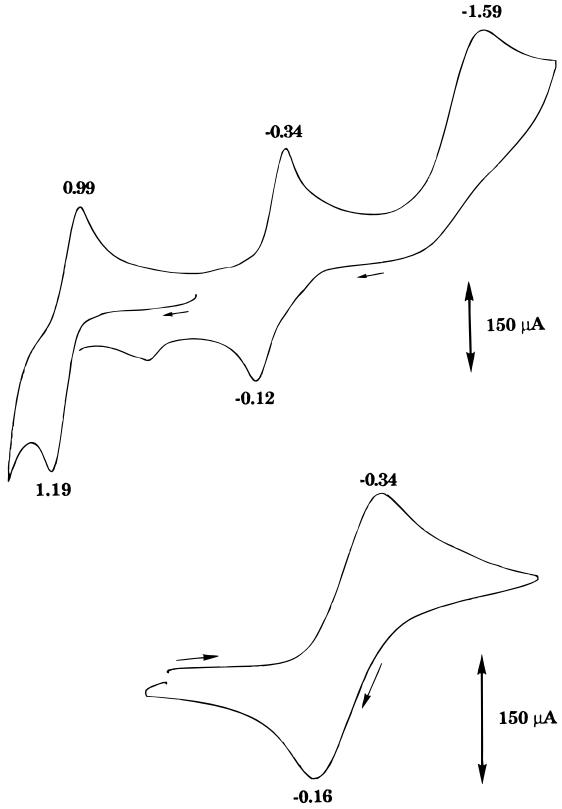

Figure 12. Cyclic voltammogram at 100 mV/s for **2** (1.0 mM) in CH_2Cl_2. The bottom scan emphasizes the reversibility of the first reduction. Potentials are vs ferrocene/ferrocenium.

processes, the i_f/i_r ratios are ∼1 and plots of i_f vs $\nu^{1/2}$ are linear in the scan rate (ν) range of 20−200 mV/s, indicating diffusion-controlled processes. The peak separations for the reversible oxidation (200 mV) and reduction (180 mV) in Figure 12 may seem large but they are comparable with the ferrocene/ferrocenium one-electron couple under the same conditions (190 mV). Complex **4** shows only irreversible processes.

Complexes **2** and **3** are thus members of the electron-transfer series defined by eq 7, which includes the potentials for **2**. On

$$\underset{2Mn^{III},2Mn^{IV}}{[\ ]^+} \overset{1.09\ V}{\rightleftharpoons} \underset{3Mn^{III},Mn^{IV}}{[Mn_4O_3X(OAc)_3(dbm)_3]} \overset{-0.25\ V}{\rightleftharpoons} \underset{4Mn^{III}}{[\ ]^-} \overset{\sim -1.5\ V}{\longrightarrow} \underset{Mn^{II},3Mn^{III}}{[\ ]^{2-}} \quad (7)$$

the electrochemical time scale at least, the $[Mn_4O_3X]$ core is stable in three oxidation levels spanning $4Mn^{III}$ to $2Mn^{III},2Mn^{IV}$. Controlled-potential electrolyses experiments on these and a variety of other Mn_4 species are currently in progress in an attempt to isolate oxidized and reduced species and assess the level of structural similarity or difference with the parent compound.[24a]

It is interesting to note that the potential of the $4Mn^{III}$/$3Mn^{III},Mn^{IV}$ couple (−0.25 V for **2**) is significantly more negative than for the same process in the $[Mn_4O_2]^{8+}$-containing complexes such as **1** (+0.61 V in CH_2Cl_2), $(NBu^n_4)[Mn_4O_2(O_2CPh)_7(dbm)_2]$ (+0.48 V in MeCN), and $(NBu^n_4)[Mn_4O_2(O_2CPh)_8(dbm)]$ (+0.33 V in CH_2Cl_2), which also contain dbm.[24b] These data demonstrate the dramatic stabilization (by ≥570 mV) of a higher oxidation state Mn_4 complex by inclusion

(22) (a) Wemple, M. W.; Adams, D. M.; Folting, K.; Hendrickson, D. N.; Christou, G. *J. Am. Chem. Soc.* **1995**, *117*, 7275. (b) Wang, S.; Tsai, H.-L.; Hagen, K. S.; Hendrickson, D. N.; Christou, G. *J. Am. Chem. Soc.* **1994**, *116*, 8376.

(23) Wemple, M. W.; Adams, D. M.; Hagen, K. S.; Folting, K.; Hendrickson, D. N.; Christou, G. *J. Chem. Soc., Chem. Commun.* **1995**, 1591.

(24) (a) Claude, J. P.; Christou, G., work in progress. (b) Wang, S.; Tsai, H.-L.; Huffman, J. C.; Folting, K.; Hendrickson, D. N.; Christou, G., manuscript in preparation.

of a third O^{2-} bridge and an X^- ion, i.e., the $[Mn_4O_3Cl]$ vs $[Mn_4O_2]$ cores.

Discussion

The reactions of the $4Mn^{III}$ complex **1** with Cl^- in hot MeCN or Me_3SiCl in CH_2Cl_2 provide convenient synthetic access to the new complex **2** *via* a disproportionation reaction. The yields are good, and the purity of the product is high. Use of Me_3SiBr in CH_2Br_2 provides an equally convenient route to the Br^- analogue **3**. The mechanisms of these reactions are undoubtedly complex, probably involving a variety of species in equilibrium in solution, and the successful isolation of **2** and **3** in satisfactory purity is likely due to their low solubility, which causes them to crystallize out from the reaction solution. Complex **4**, formed by a slightly modified version of the procedure that originally gave $Mn_4O_3Cl_4(OAc)_3(py)_3$,[10] is a very rare example of a charged $[Mn_4O_3Cl]^{6+}$ complex. We had hoped that it might have increased solubility, allowing more detailed studies in solution, but this was not the case, probably due to the extensive hydrogen bonding between the anion and the pyH^+ cations and the consequent tight ion pairing.

The preparation of complexes **2** and **3** provides the first examples of the $[Mn_4O_3X]^{6+}$ ($X = Cl^-$, Br^-) in a totally O-based ligation environment. In this regard, the ligation is now more biologically relevant to that about the WOC of PSII than was that in complex **6** and related Cl^--rich species, including **4**.[1,2] Comparison of **2** with **3**, and of **2**/**3** with previous $[Mn_4O_3Cl]^{6+}$ species and **4** allows a number of conclusions to be reached:

1. The chelate group dbm^- is resistant to oxidation by the higher oxidation state $Mn^{III/IV}$ centers in **2** and **3** and is thus able to provide stable complexes without terminal Cl^- groups at the Mn^{III} ions.

2. The incorporation of dbm^- groups in **2** and **3** in place of the terminal Cl^-/py groups of, e.g., **6**, leads to complexes that exhibit *reversible* oxidation and reduction processes when studied by electrochemical methods. Complexes **4**, **6**, and related species show only very irreversible redox behavior, possibly due to the greater lability of Cl^-/py groups compared with chelating dbm^- that allows subsequent degradative processes to occur. Complexes **2** and **3** therefore demonstrate that the $[Mn_4O_3X]^{z+}$ core can exist at three oxidation levels, *viz.* $4Mn^{III}$ ($z = 5$), $3Mn^{III}Mn^{IV}$ ($z = 6$; as isolated), and $2Mn^{III}$, $2Mn^{IV}$ ($z = 7$). Generation, isolation, and structural characterization of complexes at the other two oxidation levels now become feasible and important objectives of future work.[24a]

3. Substitution of Br for Cl has minimal effect upon the structural properties of the complexes, other than the small changes expected for the larger halide. Further, there are almost insignificant changes to the spectroscopic, electrochemical and magnetic properties of **2** on Br-for-Cl substitution; clearly, the electronic structure of these complexes is dominated by the $[Mn_4O_3]$ portion of the core. From a magnetic viewpoint, it is already known from earlier studies on previous $[Mn_4O_3Cl]^{6+}$ species (e.g., **6**)[10,25] that the exchange interaction between the $Mn^{III}\cdots Mn^{IV}$ pairs ($J = J_{34}$) dominates the $Mn^{III}\cdots Mn^{III}$ ($J' = J_{33}$) interaction: the Br-for-Cl substitution, which would be expected to affect J_{33} more than J_{34}, does not significantly affect the electronic structure of the core. This further suggests that the σ-superexchange pathway involving the X^- ions and the singly-occupied Mn^{III} d_z^2 magnetic orbitals (taking the $Mn^{III}-X$ directions as the *z* axes) is not the dominant pathway controlling the $Mn^{III}\cdots Mn^{III}$ exchange interactions, presumably because the X^- ions lie on JT elongation axes that decrease overlap between σ- (and π-) symmetry orbitals on the Mn^{III} and X^- atoms. Thus, superexchange pathways involving the oxide bridges would appear to control the $Mn^{III}\cdots Mn^{III}$ (and $Mn^{III}\cdots Mn^{IV}$) exchange interactions. The incorporation of *only* terminal Cl^- ions at the Mn^{III} ions (complex **4**) again causes only minor changes to the properties of the complex.

The characterization of **2**, **3**, and **4** brings to an end one aspect of our study of the magnetic properties of $[Mn_4O_3X(O_2CR)_3L_6]$ complexes with the distorted-cubane core of C_{3v} symmetry; we have now varied X (Cl, Br), R (Me, Et, Ph, substituted Ph), and L (three Cl/3 py, five Cl/HIm, six Cl, three dbm, where HIm is imidazole).[10,11] The structures of the cores of these various complexes are approximately invariant, as are the magnetic properties, which are dominated by the oxide bridges. As a result, all these complexes have well-isolated $S = 9/2$ ground states, with the small changes to J_{33} and J_{34} as a function of X, R, and L affecting only the precise energy separations to the excited states. What *are* dramatically affected, however, are the redox properties of the complexes, which are sensitive to the peripheral L ligands: **2** and **3** are the only ones to support reversible redox properties, emphasizing the importance of the peripheral ligation to the ability of Mn_4O/RCO_2^- clusters to adopt multiple oxidation states; this is clearly of importance to the continuing attempts to understand the WOC, a multielectron redox system, and to devise and synthesize an accurate structural and functional model. Complexes **2** and **3** also provide a clear demonstration that Br^- can substitute for Cl^- in a tetranuclear $Mn/O/RCO_2$ aggregate without affecting structural properties or redox potentials, and this is of interest when compared with the recognized ability[1,2] of Br^- to support O_2 evolution by the WOC in place of Cl^-. Presumably, the structure and the redox capability of the WOC are two of the most important parameters affecting the activity of this multielectron, biological redox catalyst. The present work provides a precedent for believing that Br^- can both structurally substitute for Cl^- (i.e., allow maintenance of the same architecture of the WOC as obtains with Cl^-) and support the same redox changes at essentially equivalent potentials that are necessary for oxygen evolution.

The $S = 9/2$ ground state possessed by the $[Mn_4O_3X]^{6+}$ complexes contrasts with the $S = {}^1/_2$ or ${}^5/_2$ EPR signals exhibited by the WOC in its S_2 oxidation level.[1,2,26−28] Our systematic variation of peripheral bridging RCO_2^- and terminal L groups, as well as bridging ion X, has now demonstrated that perturbations to the C_{3v} symmetry $[Mn_4O_3]$ subcore are required before a change in ground state *S* value might prove possible. The precise structure of the WOC is currently uncertain, and our present and previous work demonstrates that if the $[Mn_4O_3X]$ complexes are structurally related to the Mn_4 aggregate of the WOC, then the latter must have a $[Mn_4O_3]$ core that is more distorted by environmental effects than is observed in our high-symmetry model complexes. Such distortions to the $[Mn_4O_3]$ core (which need not be large in an absolute sense) that involve changes to the Mn−O−Mn angles could significantly affect the various exchange parameters that determine the ground-state, and provide a feasible means by which the ground state *S* value could conceivably change.[10,11] A more detailed consideration of how ground state *S* might vary in such lower-symmetry Mn_4 units (i.e., severely distorted versions of the $[Mn_4O_3X]$ unit) will be provided in the next paper in this series involving the properties of a new family of $[Mn_4O_3]^{7+}$ complexes.[22,24b]

(25) Schmitt, E. A.; Noodleman, L.; Baerends, E. J.; Hendrickson, D. N. *J. Am. Chem. Soc.* **1992**, *114*, 6109.
(26) Haddy, A.; Dunham, W. R.; Sands, R. H.; Aasa. R. *Biochim. Biophys. Acta* **1992**, *1099*, 25.
(27) Casey, J. L.; Sauer, K. *Biochim. Biophys. Acta* **1984**, *767*, 21.
(28) Zimmermann, J.-L.; Rutherford, A. W. *Biochim. Biophys. Acta* **1984**, *767*, 7507.

Of course, the face-capped trigonal-pyramidal $[Mn_4O_3]$ unit is only one of the topological possibilities suggested by DeRose *et al.* as being consistent with EXAFS data.[6d] Indeed, the topology favored by EXAFS authors is a "dimer-of-dimers" structure involving a more "open" or extended arrangement of two $[Mn_2(\mu\text{-}O)_2]$ units. While it may be favored on EXAFS grounds, the dimer-of-dimers model also suffers from a difficulty in rationalizing the $S = {}^5/_2$ state ($g = 4.1$ EPR signal) of the WOC at the S_2 level.[26] Solomon, Armstrong, and co-workers, in their report[29] of the magnetic properties of $[Mn_2O_2(tphpn)]_2^{4+}$, have warned of the difficulty in explaining how such a dimer-of-dimers arrangement could yield the $S = {}^5/_2$ S_2 state of the WOC that is responsible for the $g = 4.1$ EPR signal. Similarly, Girerd and co-workers, in their analysis of the complex $[Mn_4O_6(bpy)_6]^{4+}$ with an extended $[MnO_2MnO_2MnO_2Mn]$ conformation,[30] have concluded that the only way to achieve a $S = {}^5/_2$ ground state would be to have (i) (unprecedented) ferromagnetic couplings within a $[Mn_2(\mu\text{-}O)_2]^{4+}$ unit or (ii) (also unprecedented) strong ferromagnetic interactions between the two outermost Mn ions of the extended Mn_4 unit. These authors warned that it is not clear how ferromagnetic interactions could arise in a $[Mn(\mu\text{-}O)_2Mn]^{3+,4+}$ unit. The other topological possibilities consistent with EXAFS data are not known in model complexes in discrete form at the biologically relevant oxidation levels ($\geq$III), and their magnetic properties cannot therefore be assessed at the present time.

In summary, it appears fair to say that at the present time there is no theoretical structure or known synthetic complex that can be thought of as an exact model of the WOC, i.e., that is consistent with *all* the combined EXAFS, magnetic, EPR, and other known properties of this complicated biological metallosite. The $[Mn_4O_3X]$ aggregates are one of the only very few tetranuclear complexes reasonably consistent with EXAFS data that have been prepared, and as such we believe their continued study to be warranted, including their use to investigate the sensitivity of electronic structure and other properties of Mn_4 clusters to changes in environmental influences and core symmetry (distortion).

Future work is directed toward more significant perturbations of the $[Mn_4O_3X]^{6+}$ core, including its isolation at other oxidation levels or with a more distorted core, and preparing versions where X is F (an inhibitor of the WOC), other small anions, or absent altogether. Preliminary results along these directions have recently been communicated.[22,23]

Acknowledgment. This work was supported by NIH Grants GM 39083 (G.C.) and HL 13652 (D.N.H.). We thank M. W. Wemple for assistance with figure preparation.

Supporting Information Available: Complete listings of crystallographic data, fully labeled figures, bond lengths and angles, and thermal parameters for complexes **2**−**4** (48 pages). Ordering information is given on any current masthead page.

IC9601347

(29) Kirk, M. L.; Chan, M. K.; Armstrong, W. H.; Solomon, E. I. *J. Am. Chem. Soc.* **1992**, *114*, 10432.
(30) Philouze, C.; Blondin, G.; Girerd, J.-J.; Guilhem, J.; Pascard, C.; Lexa, D. *J. Am. Chem. Soc.* **1994**, *116*, 8557.